07

# Laser-induced plate-lamel graphitised structures in cvd diamond as promising radiation sensors

© A.O. Kucherik,[1] T.V. Kononenko,[2] V.D. Samyshkin,[1] A.S. Chernikov,[1] A.V. Kharkova,[1] D.N. Bukharov[1]

[1] Vladimir State University,
600000 Vladimir, Russia
[2] Prokhorov Institute of General Physics, Russian Academy of Sciences,
119991 Moscow, Russia
e-mail: buharovdn@gmail.com

*Received March 22, 2025*
*Revised July 14, 2025*
*Accepted July 21, 2025*

A controlled laser method for synthesizing plate-like graphitized structures in CVD diamond is proposed. These structures are promising as sensor surfaces for detecting charged particles that make up radiation. A model of the structure of such plates is proposed based on the diffusion approximation. Possible ways of using the obtained structures in sensor devices are proposed.

**Keywords:** laser graphitization, sensor structures, CVD diamond, plate structures, modeling, diffusion approximation.

DOI: 10.61011/TP.2026.01.62850.43-25

## Introduction

Today, materials based on artificial CVD-diamonds (Chemical Vapor Deposition) are a promising element base of modern microelectronics [1]. Thus, they are successively applied as sensor elements in various systems designed to monitor and adjust a state of important technical and industrial facilities [2–5] as well as a state of the environment [6,7].

The main advantage of these sensors it that they can function in extreme conditions: at the high temperature, pressure, in conditions of hard radioactive emissions [8–10] as well as their fast response and miniature size of sensitive elements, which makes it possible to obtain quite strong detecting signals.

One of the successful fields of using these sensors is radiation monitoring [11–13].

This sensor is based on a structure that is sensitive to radioactive particles and is a graphitized area of artificial diamond with a well developed surface. The surface can let in high-energy particles with their subsequent generation of free carriers that create an electric pulse in an external circuit, which allows measuring a total induced charge, whose value can be used to identify detected radiation. Then, the obtained signal can be transmitted to an amplifying electric circuit and an element designed to transform and normalize the output signal and to make it possible to eliminate accumulate errors and classify the obtained signals using various machine learning methods and artificial intelligence [14].

Thus, circuits of the sensors based on the graphitized area in CVD-diamonds can be a good alternative to sensor devices implemented by the standard methods.

## 1. Laser diagram of synthesis of the sensitive element of the sensor based on a graphitized plate in CVD-diamond

There is some methods of manufacturing radiation sensors based on the graphitized areas [15].

They can include a method of local laser graphitization, which is different from standard approaches by a high synthesis rate, universality, manufacturability and a capability of flexible control of parameters [16]. This method makes it possible to form lamellar graphitized structures with a regular surface [15,16] with required electrophysical properties.

In accordance with a principal diagram of local laser modification, which is shown in Fig. 1, we have synthesized the lamellar graphitized structures in a sample of synthetic CVD-diamond of the size $5 \times 5 \times 1$ mm, which was provided by CG „Diamond Valley“ (the city of Karabanovo, Russia).

CVD-diamond was exposed to pulse radiation of duration of $\tau = 550$ fs from an optical fiber laser Huaray with a Gaussian beam profile at the wavelength of $\lambda = 1.03\,\mu$m. A laser beam reflected from a narrow-band mirror was vertically falling to an aspherical lens with the focal distance of 4.5 mm. Radiation was focused in a subsurface layer of a diamond lower facet (the lattice plane (100)). Upward motion of the source as well as horizontal displacement (leftward-rightward) of the position table during exposure made it possible to form the lamellar graphitized structures. The focus was moved upwards at the speed of $1\,\mu$m/s, while values of the speed of table motion were from 20 to $200\,\mu$m/s. A frequency of laser radiation pulses

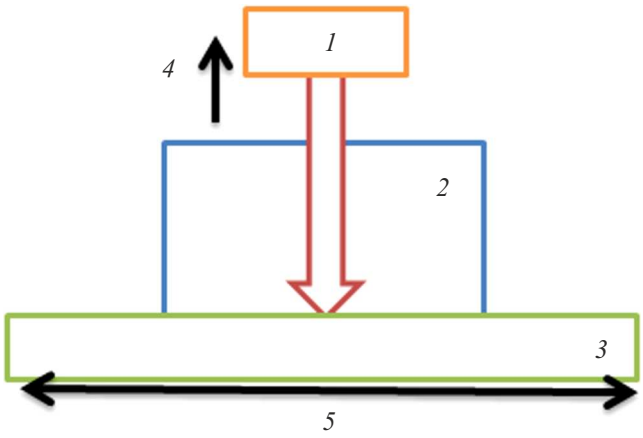


**Figure 1.** Diagram of laser modification of artificial diamond: *1* — a laser radiation source, *2* — CVD-diamond, *3* — a position table, *4* — a direction of motion of the laser radiation source, *5* — a direction of motion of the position table.

was 1 kHz, while pulse energy varied from 0.3 to 2.08 $\mu$J. For the focused beam of the diameter of 1 $\mu$m (by the level of intensity $1/e^2$), the values of the energy flux density ranged from 76 to 530 J/cm$^2$.

The said values of parameters of the synthesis diagram provided an excess of an optical breakdown threshold [17] at the rear surface.

## 2. Investigation of structural specific features of the graphitized lamellar structures

Varying the parameters of an experimental diagram (the speed of displacement of the position table and pulse energy) made it possible to synthesized the graphitized lamellar microstructures, extending a set of structures with various (filamentary and narrow band-like) topological specific features within a diamond volume [17,18]. Thus, it can be stated that the parameters of the speed of displacement of the position table and pulse energy are governing parameters of the diagram of laser synthesis of the graphitized lamellar areas in CVD-diamond.

Thus, based on the data shown in Fig. 2, it is possible to estimate the influence of a value of pulse energy on the structure of the graphitized lamellar areas. The value of laser pulse energy $E$ varied from 0.3 to 2.08 $\mu$J, when a value of the speed of horizontal displacement of the position table $v_x = 100\,\mu$m/s, a repetition rate of laser pulses $\nu = 1$ kHz as well as a focus upward displacement speed $v_z = 1\,\mu$m/s were fixed.

It is obvious from Fig. 2 that as pulse energy increased, a degree of filling of the graphitized lamellar area increased. A number of diamond inclusions was decreasing. This nature was matched with an increase of fractal dimensionality calculated by a boxcounting method [19] in the MATLAB environment (Fig. 3). The obtained dependence can be approximated by a logarithmic function of the following kind

$$D(E) = 0.0693 \ln(E) + 1.8048, \qquad (1)$$

obtained by the least-square method realized in the MATLAB environment.

The obtained values of the fractal dimensionalities confirm an increase of the area of the synthesized graphitized lamellar areas and, consequently, development of their surface.

Besides, as pulse energy increased there was observed enhancement of a degree of cracking of the diamond structure around the lamellar area. Boundaries have cracks of the length of up to 10–15 $\mu$m being formed.

Thus, obtaining well-formed homogeneous lamellar areas requires to use quite powerful pulses taking into account possible cracking at structure boundaries, when a distance between adjacent samples shall exceed two crack lengths.

An increase of the speed of motion of the position table affects a structure and topology of the lamellar structure (Fig. 2, 4). When affecting by a pulse with relatively high energy from our considered range (2.08 $\mu$J), with an increase of the speed, samples with extensive diamond inclusions are generated (Fig. 2 — the sample *1*, Fig. 4, *a*). In case of relatively low-energy effects (0.7, 0.3 $\mu$J), there is generation of the lamellar structures with multiple fine diamond inclusions, with a structure that can be represented as multiple graphitized threads.

Phase transformations that are typical for laser-induced graphitized lamellar structures were studied using Raman scattering (RS) spectroscopy. RS spectra were measured in back-scattering geometry in a mode of two-dimensional point-to-point mapping by means of an RS spectroscopy from an NTEGRA Spectra probe nanolaboratory (NT-MDT, Russia). A radiation source was a laser with the wavelength of 473 nm, the laser beam was focused by means of a 100× lens with the numerical aperture N.A. = 0.7, and a diffraction grating of 1800 strokes/mm was used in the measurements. In the mapping mode, a scanning area was a square with a side of 50 $\mu$m, an interval between adjacent points of the measurement was about 0.8 $\mu$m, and a point's exposure time was 1000 $\mu$s. Fig. 5 shows optical images and maps of distribution of intensity of an RS-signal for unmodified diamond and portions of the graphitized structures (they correspond to the samples, whose images are shown in Fig. 4), which go out to a diamond facet, near which a process of bulk modification started, as well as local-maximum-normalized RS-spectra corresponding to various points (marked with digits on the distribution maps and the optical images) of a modification area. We have considered both points close to a diamond–graphite interface (the points *1–3* in Fig. 5, *a*, the points *1, 2* in Fig. 5, *b*) as well as points closer to the center (the point *3* in Fig. 5, *b*, the points *2, 3* in Fig. 5, *c*) of the graphitization area as well as points on narrow portions with predominance of a diamond substance (the point *1* in Fig. 5, *c*).

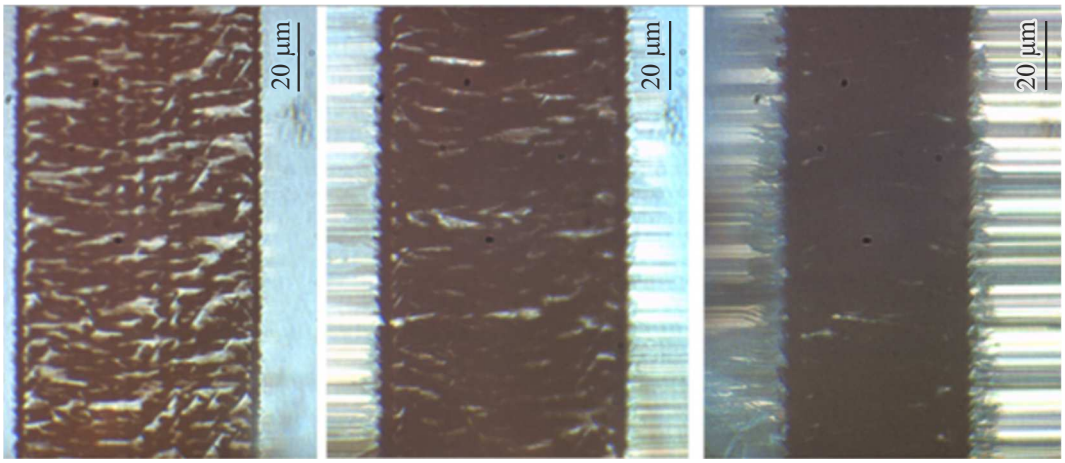


**Figure 2.** Optical images of the filamentary structures for various laser pulse energies $E$: 0.3 (*1*), 0.7 (*2*), 2.08 μJ (*3*).

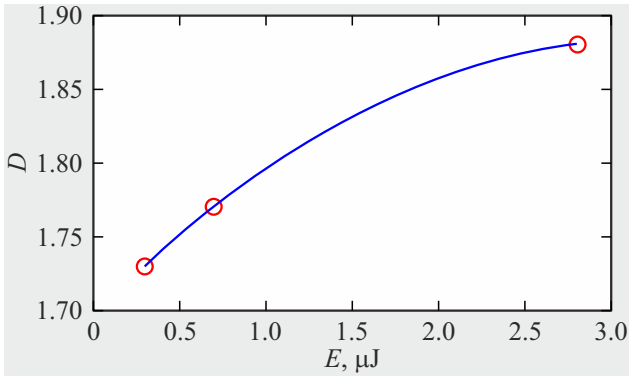


**Figure 3.** Dependence of fractal dimensionality $D$ on laser pule energy $E$ for the structures shown in Fig. 2.

On the RS-signal intensity distribution maps, portions that are red, yellow and green (high intensity) correspond to a surface of laser-unmodified diamond. In this case, the RS-spectra exhibit one intense narrow peak at $\sim 1332\,\mathrm{cm}^{-1}$ (not shown in the figure), which is a typical vibrational mode of a diamond's crystal lattice [20]. In case of portions of the graphitized structures, which go out to a diamond facet, near which a process of structure growth in the volume started (the blue color in the intensity distribution maps), wide peaks appear at $\sim 1350\,\mathrm{cm}^{-1}$ (a „disorder" ($D$) peak related to disordering of the crystal lattice) and at $\sim 1580\,\mathrm{cm}^{-1}$ (a „graphite" ($G$) peak related tensioning of C−C-bonds in graphite-like structures) [21]. At the same time, the peak at $\sim 1332\,\mathrm{cm}^{-1}$ can be retained or totally absent (the digits denote the RS-spectra taken at various points marked at the intensity distribution maps and the optical images). When comparing the RS-spectra shown in Fig. 5, one can notice certain differences in a shape of the peaks and their intensity. It indicates a heterogeneous nature of the formed structure that go out to the diamond facet and, therefore, a partial or complete transition from $sp^3$-hybridization into $sp^2$-hybridization under the effect of laser radiation. The given wide peaks at $1580\,\mathrm{cm}^{-1}$ are typical for ordered graphite, which makes it possible to assume that a graphite phase can consist of quite big cluster with limited damage of the crystal structure. A ratio of intensities for the diamond and graphite peaks can be used for estimating average sizes of the carbon cluster [22]. Intensity of the diamond peak in case of the modified surface and intensity of the signal received from an initial surfaced were compared to show reduction of intensity of the diamond peak by about 50 %.

All the three samples in Fig. 5 exhibited explicit peaks at $1580\,\mathrm{cm}^{-1}$, which indicated that micromodified areas (the points *2* and *3*) had the graphitized structures formed. In addition, the explicit peaks at $1320\,\mathrm{cm}^{-1}$ demonstrated presence of the diamond phase at boundaries of the graphitized areas. This pattern assumed that a bond $sp^3$ is transformed into a bond $sp^2$. Comparatively low intensity of the peaks at $1320\,\mathrm{cm}^{-1}$ demonstrated presence of a mixed phase of amorphous carbon at portions close to boundaries of a laser effect area. Thus, Fig. 5, *b*, c for the points *1* shows cases of a low concentration of the mixed substance and a higher concentration of the diamond component as compared to the points *2* and *3* in the same figures.

Thus, controlling the synthesis parameters (pulse energy $E$, the speed of motion of the precision table $v_x$) makes it possible to synthesize the samples with the developed structure and the required properties.

## 3. Simulation of the structure of the graphitized lamellar areas

In the first approximation, for selecting graphitization models, we will apply an imitational phenomenological approach [23] that makes it possible to describe the structure of a real sample taking into consideration only basic defining processes.

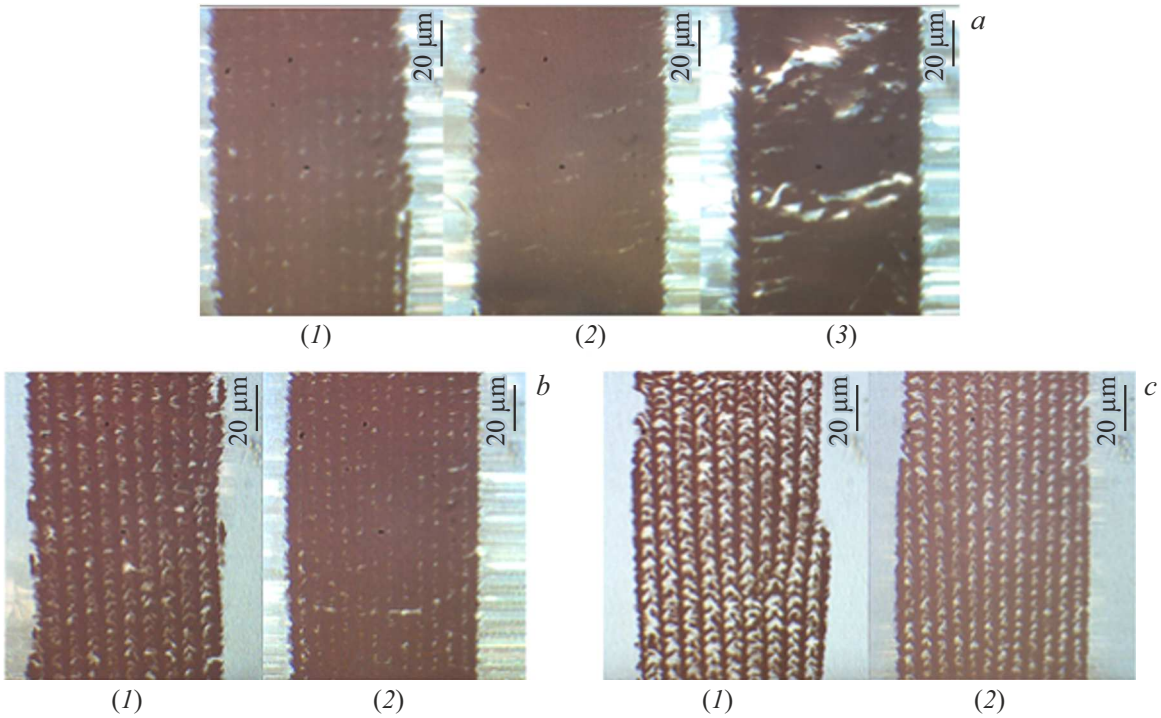


**Figure 4.** Optical images of the lamellar structures, which are obtained at the various $E$ and with varying the focus speed: *a* — $E = 2.08\,\mu$J, $v_x = 20\,\mu$m/s (*1*), $v_x = 50\,\mu$m/s (*2*), $v_x = 200\,\mu$m/s (*3*); *b* — $E = 07\,\mu$J, $v_x = 20\,\mu$m/s (*1*), $v_x = 50\,\mu$m/s (*2*); *c* — $E = 03\,\mu$J, $v_x = 20\,\mu$m/s (*1*), $v_x = 50\,\mu$m/s (*2*).

Dynamics of the laser modification process of artificial diamond during synthesis of the graphitized area is studied to demonstrate that the defining process is origination of microcracks with many „activation centers", which initiate propagation of a thermo-stimulated graphitization wave into a surrounding volume of diamond [24]. It is obvious that a process of propagation of a thermal wave that causes graphitization of areas in diamond is diffusional.

Thus, a first-approximation model describing the graphitization process can be generally represented within the framework of a diffusion equation [25,26] in a discrete case taking into account thermal factors. In this regard, the simulated system can be generally represented as a solution of the Cauchy problem, wherein a model equation is considered to be a two-dimensional diffusion equation for concentrations of the graphitized substance $u(x, y, t)$, which is supplemented with an initial condition, i.e. an initial concentration of the graphitized substance $u$:

$$\frac{\partial}{\partial t} u(x, y, t) = \nabla\big(d(x, y, t)\Delta u(x, y, t)\big), \qquad (2)$$

$$u(x, y, 0) = u_0(x, y), \qquad (3)$$

where $d(x, y, t)$ is a normalized diffusion constant.

The main model parameter that allowed taking into account thermal factors was the normalized diffusion constant. The diffusion equation was considered in a discrete form on a rectangular calculation area with a superimposed uniform grid that was forming a cell system and was solved using a cellular automaton [27] for a first-order Neumann neighborhood (Fig. 6).

It was simulated in arbitrary units (a.u.). A discretized model system was a set of cells with two states: the value 0 marked the free cell, so did 1 the graphitized cell. The initial condition was a starting distribution of already graphitized areas, which is represented by a straight line at a lower boundary of the calculation area. The graphitized structure was simulated during an iteration process of replacement of one's own state by the cells of the calculation area based on a two-rule system. First of all, the current cell was changing its state from the free to graphitized (from the marker 0 to 1) provided that its surrounding cells in the Neumann neighborhood had been already graphitized. Secondly, this state was replaced with probability typical for the cell in question ($s$). This probability ($s$) meant a normalized diffusion constant that depended on the temperature ($T$) of the considered cell of the calculation area. Then $s$ was estimated as

$$s = \gamma T/S, \qquad (4)$$

where $S$ is an area of the calculation area, $\gamma = 1/t$ is a scale coefficient, $t$ is a number of iterations.

Thus, the temperature relationship that depends on the speed of motion and pulse energy makes it possible to carry out a correspondence of parameters of the model and the real laser diagram.

In the first approximation, this correspondence can be realized, for example, based on solving a Rosenthal thermal conductivity equation [28] taking into account average

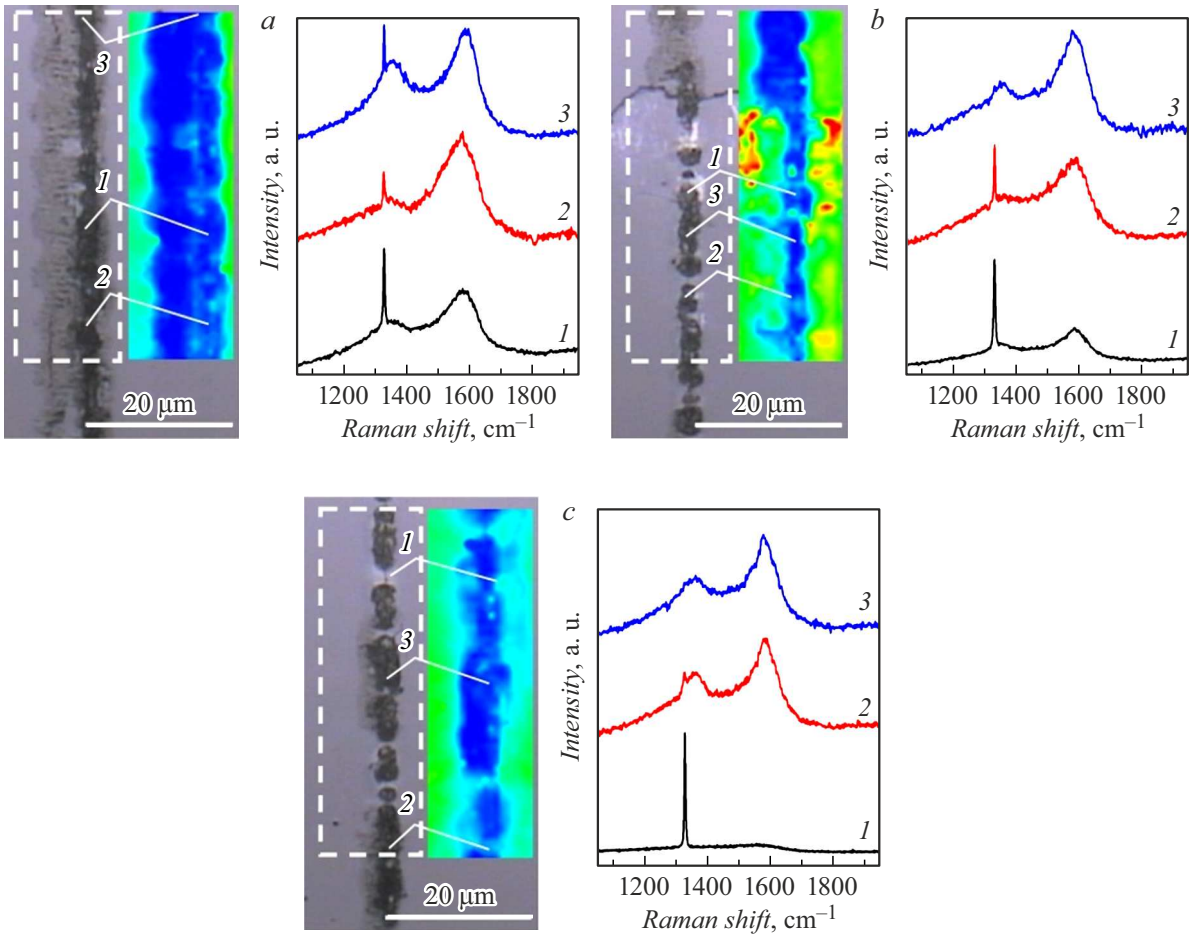


**Figure 5.** Optical images and maps of distribution of intensity of the RS-signal for unmodified diamond and the portions of the graphitized structures, which go out to the diamond facet (the left fragments), the local-maximum-normalized RS-spectra (the right fragments) corresponding to the various points (marked with digits on the RS-signal intensity distribution maps and the optical images) of the modification area: the sample *1* in Fig. 4, *a* (*a*); the sample *1* in Fig. 4, *b* (*b*); the sample *1* in Fig. 4, *c* (*c*).

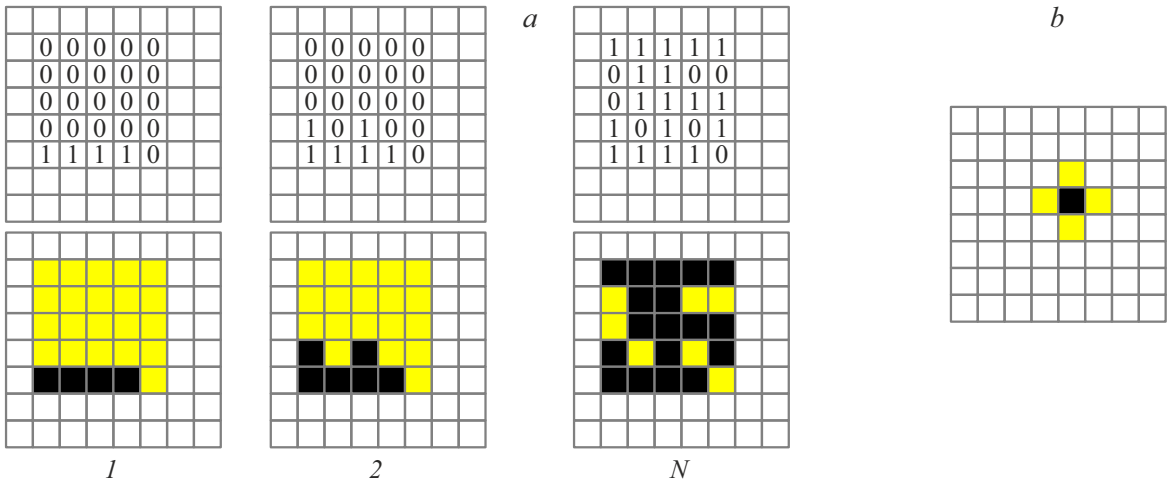


**Figure 6.** Model of the graphitization area (*a*). Diagram of 1-N iteration: above — the marked system: 1 — a graphitized cell, 0 — a free cell; below — the respective color marking; *b* — Neumann neighborhood.

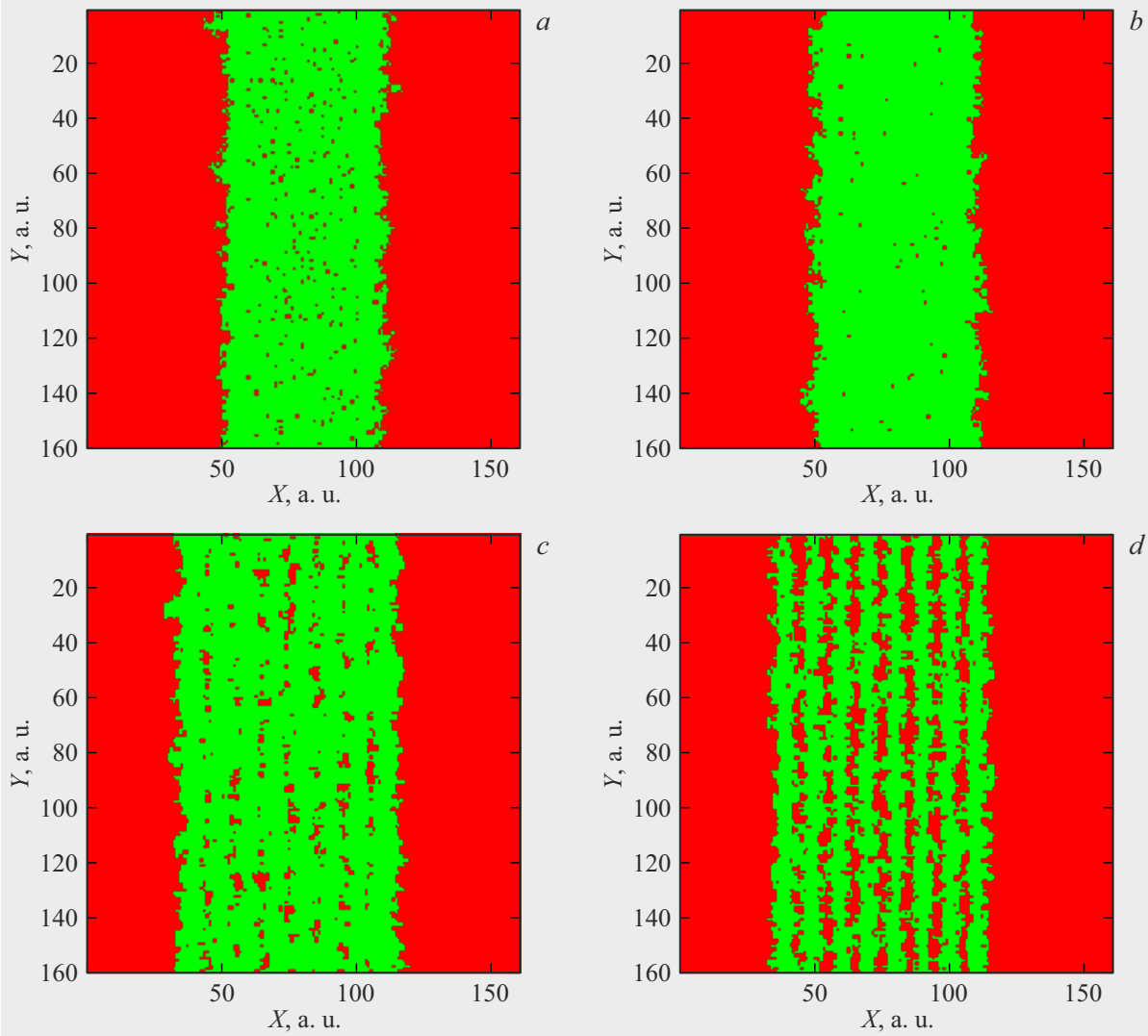


**Figure 7.** Models of side sections of the graphitized plates when varying the model parameters and at their relation with the experimental ones: $T = 5500\,^{\circ}$C, $s = 0.021$, $v_x = 20\,\mu$m/s, $E = 2.08\,\mu$J $(a)$; $T = 4000\,^{\circ}$C, $s = 0.016$, $v_x = 50\,\mu$m/s, $E = 2.08\,\mu$J $(b)$; $T = 4000\,^{\circ}$C, $s = 0.016$, $v_x = 20\,\mu$m/s, $E = 0.3\,\mu$J $(c)$; $T = 4000\,^{\circ}$C, $s = 0.016$, $v_x = 50\,\mu$m/s, $E = 0.3\,\mu$J $(d)$.

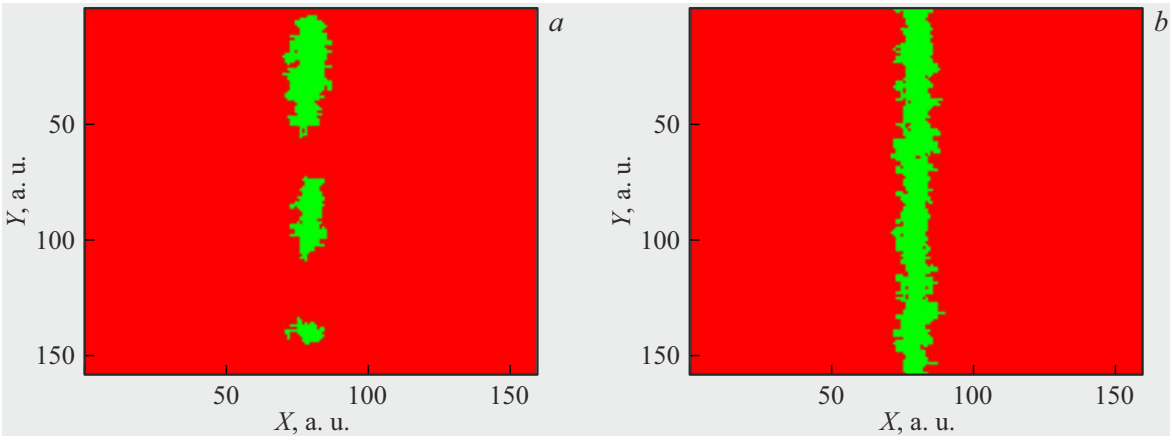


**Figure 8.** Models of surfacing of the graphitized plate: $a$ — for the case of low-energy effect, $b$ — for the case of high-energy effect.

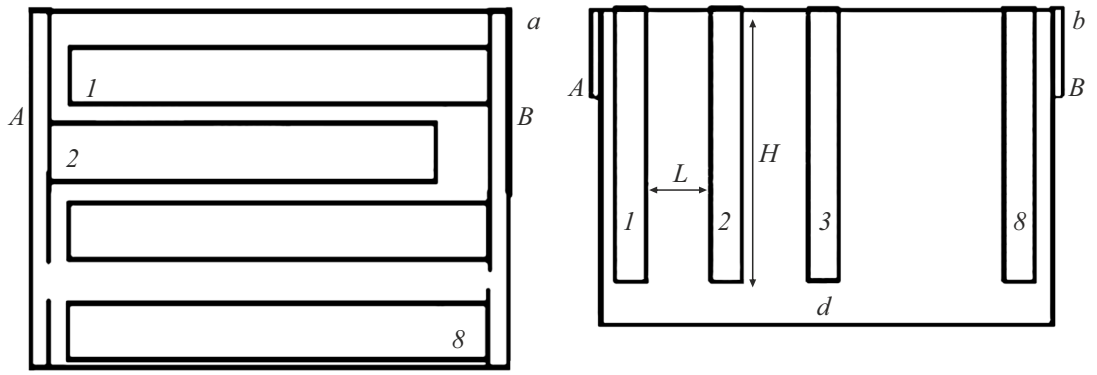


**Figure 9.** Principal diagram of the eight-channel sensor surface for detecting the high-energy particles: a plan view ($a$), a side view: $L = 250\,\mu$m, $H = 300\,\mu$m, $d = 20\,\mu$m ($b$). The points $A$, $B$ are energized.

power of a pulse source [29] as

$$s \sim \gamma_1 E \quad \text{and} \quad s \sim \gamma_2 \exp(-\gamma_3 v_x), \tag{5}$$

where $\gamma_1, \gamma_2, \gamma_3$ are coefficients of proportionality.

The proposed model was realized in the MATLAB environment for the various temperature values in the stationary case. Thus, graphitization was realized for the temperatures 4000 °C–6000 °C [30]. Fig. 7, 8 shows models for the various parameter ratios. Fig. 7 shows a side view: Fig. 7, *a, b* corresponds to the higher-energy effect for energy values from our considered range ($2.08\,\mu$J), so does Fig. 7, *c, d* to lower-energy effect therefor ($0.3\,\mu$J).

Fig. 8 shows models of surfacing of the graphitized plates. A starting structure was selected to be a set of lines (Fig. 8, *a*) or a line in the center (Fig. 8, *b*).

A transition to absolute units made it possible to estimate sizes of model structures, which did not contradict magnitudes of the real samples.

An error of simulation was estimated for the proposed approximation by relating the fractal dimensionalities calculated by the boxcounting method. The error not exceeding 8 % was achieved, thereby indicating adequacy of the proposed approximation. Thus, the correspondence of the fractal dimensionalities of the models and the real samples make it possible to hope for noncontradiction of their electrophysical and optical functional properties [31–35].

## 4. Possible ways of using the laser-induced graphitized structures in CVD-diamond as sensor surfaces

The produced lamellar structures can be applied as sensor elements for a diamond detector based on a principle with buried laser-induced electrodes [36].

The diamond detector of ionizing radiation and elementary particles can operate according to this scheme [37]. In this detector, when hitting the sensor surface, the high-energy $\beta$-particle generates a certain number of free carriers, whose motion in the electric field forms an electric pulse.

Based on the system of the lamellar graphitized structures, a sensor surface with the buried electrodes was realized and its diagram is shown in Fig. 9.

The buried electrodes were formed of periodic mutually parallel graphitized lamellar structures that surfaced diamond. A distance between the graphitized plates was $250\,\mu$m, which made it possible to eliminate a possible effect of cracking of the diamond structure and spurious branches.

The graphitized structures were produced at pulse energy $E = 2.08\,\mu$J and at $v_x = 20\,\mu$m/s. The said values of the governing parameters made it possible to produce high-quality samples with a regular structure.

The designed sensor surface was tested using a $^{90}$Sr $\beta$-source that generated electrons with the maximum energy of 2.28 MeV.

In testing, odd and even rows were energized with a different potential that created a space-periodic electric field. Each high-energy $\beta$-particle passing through the sensor surface generated free carriers that created the electric pulse in the external circuit, which allowed measuring the total induced charge. A particle flux was located in the center of the sensor surface parallel to the buried electrodes.

Fig. 10 shows testing of the sensor surface. Fig. 10, *a* demonstrate the number of recorded electric pulses in the dependence on the charge corresponding to these pulses. The said dependence is obtained as an average value of 4 and 5 tracks, which is approximated by splines in MATLAB.

The obtained dependence makes it possible to estimate the most probable value of the collected charge as 1.78 fC as well as efficiency of collection of generated free charge carriers, which is determined by an average value of the collected charge (2.25 fC).

In the first approximation, efficiency of charge collection can be evaluated by a value of about 80 %.

Fig. 10, *b* shows a dependence of the integral number of electric pulses for the various channels of the sensors structure on a direction of incidence of $\beta$-particles to the detector, which is approximated by splines in MATLAB.

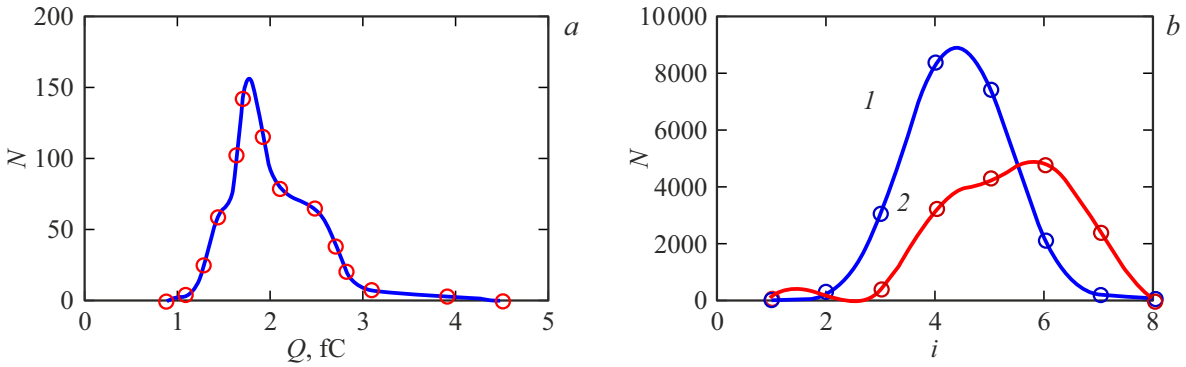


**Figure 10.** Testing the sensor surface: a dependence of a number of recorded electric pulses on the total electrical charge corresponding to these pulses (*a*), an integral number of electric pulses for the buried electrodes in a dependence on an angle of deviation of a trajectory of $\beta$-particles from a vertical direction: *1* — the vertical direction, *2* — the deviation by the angle of 20° (*b*).

Thus, when a source axis was shifted, we observed a change of the distribution. This specific feature paves the way for using the sensor surface with the buried electrodes as a detector designed to localize a source of ionizing particles.

## Conclusion

The laser effect on the samples of artificial diamonds allows controllably forming the graphitized lamellar structures with a quite developed surface, which are promising for use in various applications, in particular, as the element base for micro- and nano-electronics as well as when designing high-sensitivity sensors and detectors of a various purpose in a nanosensorics scale.

The diagram of synthesis of such graphitized diamond configurations, which is proposed in the study, is aimed at solving a task of a controllable method of laser induction of the plate samples. Varying values of the basic governing parameters of the used laser experimental diagram, such as the speed of displacement of the position table, laser pulse energy as well as the relationships between them makes it possible to produced the graphitized structures in the samples of artificial diamond with the required topological characteristics and, therefore, the electrophysical and optical characteristics governed thereby.

The proposed models of the structure of the graphitized areas showed good adequacy in a diffusion approximation and can be used for planning the experiments of controllable laser synthesis of the samples of the graphitized structures with the required properties. Thus, a relation of the parameters of the model and the synthesis diagram is arranged via a value of the system heating temperature, while the fractal dimensionality defined during simulation makes it possible to hope for similarity of the functional characteristics (optical or electrophysical ones that depend on the fractal dimensionality) of the model and the predicted sample. For example, a value of electrical conductance, whose estimation depends on a fractal dimensionality of a sensor sensitive element, affects its sensitivity. Moreover, a value of roughness of the sensitive elements also depends on the fractal dimensionality and determines attachability of molecules of the detected substance to the sensitive surface.

A prototype of the sensor surface was tested to show that the systems of the lamellar structures can be successively uses as the element base in radiation sensors.

### Funding

This study was performed under the state assignment for research of the Ministry of Science and Higher Education of the Russian Federation as part of the scientific project FZUN-2024-0018.

### Conflict of interest

The authors declare that they have no conflict of interest.

## References

[1] D. Araujo, M. Suzuki, F. Lloret, G. Alba, P. Villar. Materials (Basel), **14** (22), 7081 (2021). DOI: 10.3390/ma14227081

[2] W. Adam, E. Berdermann, P. Bergonzo, W. de Boer, F. Bogani, E. Borchi, A. Brambilla, M. Bruzzi, C. Colledani, J. Conway, P. D'Angelo, W. Dabrowski, P. Delpierre, W. Dulinski, J. Doroshenko, B. van Eijk, A. Fallou, P. Fischer, F. Fizzotti, C. Furetta, K.K. Gan, N. Ghodbane, E. Grigoriev, G. Hallewell, S. Han, F. Hartjes, J. Hrubec, D. Husson, H. Kagan, J. Kaplon, R. Kass, M. Keil, K.T. Knoepfle, T. Koeth, M. Krammer, A. Logiudice, R. Lu, L. Mac Lynne, C. Manfredotti, D. Meier, D. Menichelli, S. Meuser, M. Mishina, L. Moroni, J. Noomen, A. Oh, M. Pernicka, L. Perera, R. Potenza, J.L. Riester, S. Roe, A. Rudge, S. Sala, M. Sampietro, S. Schnetzer, S. Sciortino, H. Stelzer, R. Stone, C. Sutera, W. Trischuk, D. Tromson, C. Tuve, B. Vincenzo, P. Weilhammer, N. Wermes, M. Wetstein, W. Zeuner, M. Zoeller. Eur. Phys. J. C, **33**, 1014 (2004). DOI: 10.1140/epjcd/s2004-03-1798-6

[3] R.S. Sussmann, J.R. Brandon, S.E. Coe, J.L. Collins, A.J. Whitehead. Industrial Diamond Rev., **61**, 271 (2001).

[4] R.S. Sussmann. *CVD Diamond for Electronic Devices and Sensors* (Wiley, Chichester, 2009)
[5] H. Kagan, A. Alexopoulos, M. Artuso, F. Bachmair, L. Bäni, M. Bartosik, J. Beacham, H. Beck, V. Bellini, V. Belyaev, B. Bentele, P. Bergonzo, A. Bes, J.-M. Brom, M. Bruzzi, G. Chiodini, D. Chren, V. Cindro, G. Claus, J. Collot, J. Cumalat, A. Dabrowski, R. D'Alessandro, D. Dauvergne, W. de Boer, S. Dick, C. Dorfer, M. Dunser, V. Eremin, G. Forcolin, J. Forneris, L. Gallin-Martel, M.-L. Gallin-Martel, K.K. Gan, M. Gastal, C. Giroletti, M. Goffe, J. Goldstein, A. Golubev, A. Gorišek, E. Grigoriev, J. Grosse-Knetter, A. Grummer, B. Gui, M. Guthoff, I. Haughton, B. Hiti, D. Hits, M. Hoeferkamp, T. Hofmann, J. Hosslet, J.-Y. Hostachy, F. Hügging, C. Hutton, J. Janssen, K. Kanxheri, G. Kasieczka, R. Kass, F. Kassel, M. Kis, G. Kramberger, S. Kuleshov, A. Lacoste, S. Lagomarsino, A. Lo Giudice, E. Lukosi, C. Maazouzi, I. Mandic, C. Mathieu, M. Menichelli, M. Mikuž, A. Morozzi, J. Moss, R. Mountain, S. Murphy, M. Muškinja, A. Oh, P. Olivero, D. Passeri, H. Pernegger, R. Perrino, F. Picollo, M. Pomorski, R. Potenza, A. Quadt, A. Re, M. Reichmann, G. Riley, S. Roe, D. Sanz, M. Scaringella, D. Schaefer, C.J. Schmidt, D.S. Smith, S. Schnetzer, S. Sciortino, A. Scorzoni, S. Seidel, L. Servoli, B. Sopko, V. Sopko, S. Spagnolo, S. Spanier, K. Stenson, R. Stone, C. Sutera, A. Taylor, B. Tannenwald, M. Traeger, D. Tromson, W. Trischuk, C. Tuve, J. Velthuis, N. Venturi, E. Vittone, S. Wagner, R. Wallny, J.C. Wang, J. Weingarten, C. Weiss, T. Wengler, N. Wermes, M. Yamouni, M. Zavrtanik. Accelerators, Spectrometers, Detectors and Associated Equipment, **924**, 297 (2019). DOI: 10.1016/j.nima.2018.06.009
[6] Y. Xiaoxi, F. Yang, H. Li. *Recent Progress and Development on Nanostructures* (IntechOpen, 2024), DOI: 10.5772/intechopen.1006609
[7] B. Dischler, C. Wild. *Low-Pressure Synthetic Diamond. Springer Series in Materials Processing* (Springer, Berlin, Heidelberg, 1998), DOI: 10.1007/978-3-642-71992-9_13
[8] G.K. Samudrala, S.L. Moore, Y.K. Vohra. Materials, **8** (5), 2054 (2015). DOI: 10.3390/ma8052054
[9] A. Metcalfe, G. Fern, George, P. Hobson, P. Smith, D. Lefeuvre, G. Saenger. J. Instrumentation, **12**, 01066 (2017). DOI: 10.1088/1748-0221/12/01/C01066
[10] C. Ahl, T. Beck, E. Lukosi. Appl. Phys. Lett., **119** (25), 252103 (2021). DOI: 10.1063/5.0067578
[11] P. Bergonzo, A. Brambilla, D. Tromson, C. Mer, B. Guizard, F. Foulon, V. Amosov. Diamond Related Mater., **10** (3–7), 631 (2001). DOI: 10.1016/S0925-9635(00)00554-9
[12] A.V. Krasil'nikov, N.B. Rodionov, A.P. Bol'shakov, V.G. Ral'chenko, S.K. Vartapetov, Yu.E. Sizov, S.A. Meshchaninov, A.G. Trapeznikov, V.P. Rodionova, V.N. Amosov, R.A. Khmel'nitskii, A.N. Kirichenko. ZhTF, **92** (4), 596 (2022) (in Russian). DOI: 10.21883/JTF.2022.04.52247.226-21
[13] T. Shimaoka, S. Koizumi, J.H. Kaneko. Functional Diamond, **1** (1), 205 (2021). DOI: 10.1080/26941112.2021.2017758
[14] A. Kucherik, A. Kumar, A. Abramov, V. Samyshkin, A. Osipov, I. Bordanov, S. Shchanikov, M. Kumar. Nanotechnology, **36** (7), 072002 (2025). DOI: 10.1088/1361-6528/ad947c
[15] W. Adam, C. Bauer, E. Berdermann, P. Bergonzo, F. Bogani, E. Borchi, A. Brambilla, M. Bruzzi, C. Colledani, J. Conway, W. Dabrowski, P. Delpierre, A. Deneuville, W. Dulinski, B. van Eijk, A. Fallou, F. Fizzotti, F. Foulon, M. Friedl, K.K. Gan, E. Gheeraert, E. Grigoriev, G. Hallewell, R. Hall-Wilton, S. Han, F. Hartjes, J. Hrubec, D. Husson, H. Kagan, D. Kania, J. Kaplon, C. Karl, R. Kass, K.T. Knöpfle, M. Krammer, A. Logiudice, R. Lu, P.F. Manfredi, C. Manfredotti, R.D. Marshall, D. Meier, M. Mishina, A. Oh, L.S. Pan, V.G. Palmieri, M. Pernicka, A. Peitz, S. Pirollo, P. Polesello, K. Pretzl, V. Re, J.L. Riester, S. Roe, D. Roff, A. Rudge, S. Schnetzer, S. Sciortino, V. Speziali, H. Stelzer, R. Stone, R.J. Tapper, R. Tesarek, G.B. Thomson, M. Trawick, W. Trischuk, E. Vittone, A.M. Walsh, R. Wedenig, P. Weilhammer, H. Ziock, M. Zoeller. Accelerators, Spectrometers, Detectors Associated Equipment, **434** (1), 131 (1999). DOI: 10.1016/S0168-9002(99)00447-7
[16] C.E. Nebel. Functional Diamond, **3** (1), 2201592 (2023). DOI: 10.1080/26941112.2023.2201592
[17] T.V. Kononenko, K.K. Ashikkalieva, V.G. Ral'chenko, V.V. Kononenko, V.I. Konov. Diamond Related Mater., **142**, 110812 (2024).
[18] V.V. Kononenko, E.V. Zavedeev, T.V. Kononenko, V.V. Bukin, V.I. Konov. Diamond. Photonics, **10** (1), 43 (2023). DOI: 10.3390/photonics10010043
[19] Y. Jundong, S. Yuanyuan, C. Shanshan, H. Xiaopeng. J. Appl. Analysis Computation, **6** (4), 1114 (2016).
[20] S. Prawer, R.J. Nemanich. Philosophical Transactions Royal Society of London. Series A: Mathem., Phys. Eng. Sci., **362** (1824), 2537 (2004).
[21] A. Dychalska, P. Popielarski, W. Franków, K. Fabisiak, K. Paprocki, M. Szybowicz. Mater. Sci.-Pol., **33** (4), 799 (2015).
[22] A.A. Khomich, V. Kononenko, O. Kudryavtsev, E. Zavedeev, A.V. Khomich. Nanomaterials, **13**, 162 (2023). DOI: 10.3390/nano13010162
[23] G. Stiesch. *Modeling Engine Spray and Combustion Processes. Heat and Mass Transfer* (Springer, Berlin, Heidelberg, 2003)
[24] T.V. Kononenko, E.V. Zavedeev, V.V. Kononenko, K.K. Ashikkalieva, V.I. Konov. Appl. Phys. A, **119**, 405 (2015). DOI: 10.1007/s00339-015-9109-0
[25] A.A. Evseev, O.I. Nechaeva. PDM, **4**, 72 (2009) (in Russian).
[26] D.N. Bukharov, T.V. Kononenko, A.O. Kucherik. Pis'ma v ZhTF (in Russian), **51** (1), 26 (2025). DOI: 10.61011/PJTF.2025.01.59516.19964
[27] D.A. Zaitsev. Theoretical Computer Sci., **666**, 21 (2017). DOI: 10.1016/j.tcs.2016.11.002
[28] M. Moda, A. Chiocca, G. Macoretta, B.D. Monelli, L. Bertini. Materials Design, **223**, 110991 (2022). DOI: 10.1016/j.matdes.2022.110991
[29] B. Bhattacharyya, B. Doloi. *Modern Machining Technology Advanced, Hybrid, Micro Machining and Super Finishing Technology* (London, Academic Press, 2020), DOI: 10.1016/B978-0-12-812894-7.00004-9
[30] K.K. Ashikkalieva, T.V. Kononenko, V.I. Konov. Optics Laser Technol., **107**, 204 (2018). DOI: 10.1016/j.optlastec.2018.05.040
[31] D.N. Bukharov, A.O. Kucherik, S.M. Arakelian. J. Adv. Mater. Technol., **8** (3), 227 (2023). DOI: 10.17277/jamt.2023.03.pp.227-251
[32] D.N. Bukharov, S.M. Arakelyan, A.O. Kucherik, O.A. Novikova, V.D. Samyshkin. J. Phys.: Conf. Ser., **1439**, 012050 (2020). DOI: 10.1088/1742-6596/1439/1/012050

[33] T. Yang, F. Tian, J.A. Covington, F. Xu, Y. Xu, A. Jiang, J. Qian, R. Liu, Z. Wang, Y. Huang. Chemosensors, **7**, 31 (2019). DOI: 10.3390/chemosensors7030031
[34] A. Jiang, F. Tian, J.A. Covington, M. Jiang, Z. Wu. IEEE Transactions on Instrumentation and Measurement, **71**, 9506207 (2022). DOI: 10.1109/TIM.2022.3175026
[35] F. Tian, A. Jiang, T. Yang, J. Qian, R. Liu, M. Jianga. IEEE Sensors J., **21**, 13 (2021). DOI: 10.1109/JSEN.2021.3072621
[36] S. Salvatori, M.C. Rossi, G. Conte, T. Kononenko, M. Komlenok, A. Khomich, V. Ralchenko, V. Konov, G. Provatas, M. Jaksic. IEEE Sensors J., **19** (24), 1908 (2019). DOI: 10.1109/JSEN.2019.2939618
[37] S.O. Kasap. *Photoconductivity and Photoconductive Material* (Wiley, Chichester, 2022)

*Translated by M.Shevelev*